Author Manuscript

Author Manuscript

Author Manuscript

Author Manuscript

HHS Public Access

Author manuscript

Microcirculation. Author manuscript; available in PMC 2017 October 01.

Published in final edited form as:

Microcirculation. 2016 October ; 23(7): 558–570. doi:10.1111/micc.12307.

Macrophage alterations within the mesenteric lymphatic tissue are associated with impairment of lymphatic pump in metabolic syndrome

Scott D. Zawieja, **Wei Wang**, **Sanjukta Chakraborty**, **David C. Zawieja**, and **Mariappan Muthuchamy**

Department of Medical Physiology, College of Medicine, Cardiovascular Research Institute Division of Lymphatic Biology, Texas A&M Health Science Center, 359 Reynolds Medical Building, College Station, TX 77843-1114, USA

Abstract

The intrinsic lymphatic pump is critical to proper lymph transport and is impaired in models of the metabolic syndrome (MetSyn). Lymphatic contractile inhibition under inflammatory conditions has been linked with elevated nitric oxide (NO) production by activated myeloid–derived cells. We utilized a high fructose-fed rat model of MetSyn to test our hypothesis that inhibition of the MLV pump function in MetSyn animals was dependent on NO and was associated with altered macrophage recruitment and polarization within the mesenteric lymphatic vessels (MLV). MetSyn resulted in a greater accumulation of M1-skewed ($CD163^{+}MHCII^{+}$) macrophages that were observed both within the perivascular adipose tissue and invested along the lymphatic vessels in MetSyn rats when compared to control rats. LECs and LMCs basally express the macrophage maturation polarization cytokines monocyte colony-stimulating factor and dramatically up regulate the M1 promoting cytokine granulocyte/monocyte colony-stimulating factor in response to lipopolysaccharide stimulation. MetSyn MLVs exhibited altered phasic contraction frequency. Incubation of MetSyn MLVs with LNAME or glibenclamide had a partial restoration of lymphatic contraction frequency. The data presented here provide the first evidence for a correlation between alterations in macrophage status and lymphatic dysfunction that is partially mediated by NO and K_{ATP} channel in MetSyn rats.

Keywords

Lymphatic contractility; Macrophage polarization; Metabolic syndrome; Nitric oxide

Introduction

Proper lymphatic function is critical to tissue fluid and macromolecule homeostasis and antigen delivery to the node. Lymph must be pumped from the periphery against a net pressure gradient towards the junction of the subclavian vein and the lymphatic thoracic duct via extrinisic forces and the intrinsic contractions of lymphatic collecting vessels (78).

Corresponding author: Mariappan Muthuchamy, Ph.D., Phone: 979-436-0829; marim@tamu.edu.

Author Manuscript Author Manuscript Author Manuscript Author Manuscript

Lymphatic collecting vessels exhibit both sensitive regulation of vessel tone and also rhythmic large contractions that can be described in similar terms as the cardiac cycle (2). Physical stimuli such as shear stress (flow) and stretch (pressure) both have significant roles in the regulation of lymphatic contractions (8). In humans, the intrinsic contractions are responsible for transporting up to 2/3 of lymph from the lower extremities (14), and failure of the lymphatic system results in a chronic and progressive disease called lymphedema (53).

While genetic malformations are linked with primary lymphedema, the majority of lymphedema cases are secondary to other complications. Massive localized lymphedema (MLL) appears to be a spontaneous lymphedema within the morbidly obese population (18, 20). Obesity affects over one third of the U.S. population, is the strongest predictor of the metabolic syndrome (MetSyn) (26), and is a historical risk factor for developing secondary lymphedema in post-surgical cancer patients. Obesity and type II diabetes mellitus (TIIDM) are both associated with microvascular dysfunction (1, 47, 50, 64, 71). However, much of the focus on the peripheral edema associated with obesity has been decidedly on venous insufficiency (59, 68) with little regard to lymphatic function and its role in fluid homeostasis (12, 31, 60, 69). It is likely there is an unrecognized role for lymphatic deficiency in theses conditions as venous reabsorption is overstated (63). The association between lymphatic dysfunction and obesity becomes clear in the morbidly obese population (15, 18, 43, 49) that represent up to 29% of all secondary lymphedema cases (19).

Elevated production of inflammatory cytokines such as tumor necrosis factor alpha (TNFα), interleukin 6 (IL-6), and chemokine (C-C motif) ligand 2 (CCL2) are hallmarks of adipose inflammation, obesity, and MetSyn (10). The expression of these inflammatory cytokines is directly linked to the increased infiltration of macrophages that display the classical (M1) macrophage polarization phenotype and express high levels of iNOS (44, 45). Furthermore circulating lipopolysaccharide (LPS), an abundant dietary endotoxin, is elevated in obesity and MetSyn and is thought to contribute to the initiation of inflammation (6, 7). Under physiological conditions, adipose tissue macrophages demonstrate an alternative activated phenotype (M2) due to the expression of interleukin 4 by eosinophils (75). IFNγ is the classical stimulator of the M1 phenotype, but recent studies have also suggested that macrophage polarization can be driven by the ratio of MCSF and GMCSF (22, 32, 37). However, macrophage polarization and spatial association with the lymphatic collecting vessels has not been addressed in the context of MetSyn.

Recent studies have demonstrated a role for $CD11b^+$ myeloid-derived cells in lymphatic dysfunction (35, 41) observed in models of acute inflammation, and specifically the excessive production of nitric oxide (NO) by inducible nitric oxide synthase (iNOS) (41). NO is a critical mediator of the shear stress produced as an effect of lymph flow (23, 24) and acts as a contractility brake resulting in lower contraction frequency, vessel dilation, and ultimately reduced resistance to flow (62, 70). However, excessive NO production by myeloid derived cells has been linked to poor lymphatic function as function of repressed contraction frequency in both mouse (41) and guinea pig models of inflammation (48). Nitric oxide activates the lymphatic muscle cGMP-PKG/PKA pathway resulting in activation of ATP sensitive potassium channels (K_{ATP}) and membrane hyperpolarization

Author Manuscript Author Manuscript Author Manuscript Author Manuscript

decreasing the voltage gated calcium channels activation and spontaneous contraction (39, 48). In this study we have asked the question that whether inhibition of NOS or K_{ATP} channel would restore the lymphatic contractile function in MetSyn animals.

We have previously demonstrated a significant reduction in the intrinsic lymph pump capability of the MLV in a rat model of high fructose fed MetSyn (79). Recently, others have demonstrated a reduction in phasic activity and lymph function in genetic and diet-induced models of obesity, which also fit under the umbrella of MetSyn models (3, 61, 74). However, the mechanism underlying the inhibition of contractility is unknown. In this study we have determined how the changes in the mesenteric environment influence the macrophage recruitment and polarization in MetSyn condition. We have assessed the role of NO in the impairment of MLV contractions with the pan nitric oxide synthase (NOS) inhibitor LNAME and the anti-diabetic drug glibenclamide (Glib), a K_{ATP} channel inhibitor, on regulating lymphatic chronotropy and function in the MetSyn state.

Materials and Methods

Animal Handling

Thirty-two male Sprague-Dawley rats weighing 150–180g were ordered from Charles River for the induction of the MetSyn. Eighteen rats were given a high fructose feed (HFF) diet (60% fructose, ID.89247 Harlan Teklad®, 66% caloric content from fructose) for seven weeks to induce the MetSyn, while the remaining fourteen animals were given standard rodent chow. Water and each respective feed were available ad libitum except during pre-experiment (16hr) fasting. Twelve rats from the MetSyn group and eight rats from the control group were utilized for isobaric functional analysis of MLV contractility. The remaining six rats were used for IHC and RNA collection from the mesentery tissue. All animals were housed in a facility accredited by the Association for the Assessment and Accreditation of Laboratory Animal Care and maintained in accordance with the policies defined by the Public Health Service Policy for the Humane Care and Use of Laboratory Animals, the United States Department of Agriculture's Animal Welfare Regulations and the Scott & White Animal Care and Use Committee.

Determination of MetSyn

High fructose feeding for 7-weeks is sufficient to generate a rat model of MetSyn (54). MetSyn was assessed as previously described through the use of serum analysis (79). In short, blood was collected in fasted (16hr) rats via the lateral saphenous veins at the start and end of the diet period. The saphenous vein was punctured using a 27gauge needle and blood was collected in a non-heparinized tube. Blood was allowed to clot for 1hour at room temperature and spun for ten minutes at 3,000g. Serum was then frozen and stored at −80°C. Triglyceride and insulin concentrations were assessed using commercially available colorimetric kits, Bioassays® ETGA-200 and an insulin ELISA kit Linco® EZMRI-13k, respectively, following the manufacturers' protocols.

Author Manuscript Author Manuscript Author Manuscript Author Manuscript

MLV Isolation

Rats were fasted for sixteen hours (o/n) to minimize the variability of lymph contents or immune cell population changes in the post-prandial state. Rats were anesthetized with Innovar-Vet (0.3 ml kg-1 I.M.), which is a combination of a droperidol-fentanyl solution (droperidol 20 mg/ml, fentanyl 0.4 mg/ml), and diazepam (2.5 mg/kg IM). A midline excision was made and a loop of ileum was carefully exteriorized. Two to three MLVs were carefully dissociated from the surrounding adipose tissue with care to prevent excess bleeding. Vessels were maintained in albumin-supplemented physiological saline solution (APSS, in mM: 145.0 NaCl, 4.7 KCl, 2 CaCl2, 1.17 MgSO4, 1.2 NaH2PO4, 5.0 glucose, 2.0 sodium pyruvate, 0.02 EDTA and 3.0 3-(N-morpholino) propanesulfonic acid (MOPS) and 1% w/v bovine serum albumin) at pH 7.4 at 38°C. MLVs were then cannulated onto matched pipettes in a CH-1 chamber® (Living Systems) and attached to separate pressure reservoirs. Vessels were then allowed to reach temperature and equilibrate at pressure 3cmH_2O for approximately thirty minutes. After the equilibration period each vessel was recorded for 5 minutes at pressures 1cm, 3cm, and 7cmH_2O. Of the 8 MetSyn vessels, half were incubated with 100μM LNAME at 1cmH_2O for twenty minutes before repeating the pressure step protocol in the presence of LNAME. The remaining 4 MetSyn MLVs were recorded at each pressure after they were stimulated with 1μM Glib at each pressure following a fifteen-minute equilibration period at each concentration and then this process was repeated with 10μM Glib. At the end of each experiment the bath solution was replaced with calcium-free APSS and maximal diameter at each pressure recorded.

Isolated Vessel Video Analysis

Lymphatic diameters were traced for each 5 min video capture with a vessel wall-tracking program developed and provided by Dr. Michael J. Davis (University of Missouri-Columbia) (11). Outer lymphatic vessel diameters were tracked 30 times per second, providing a tracing of diameter changes throughout the periods of systole and diastole. The following analogies to the cardiac pump parameters were derived: lymphatic tonic index, contraction amplitude, ejection fraction, contraction frequency, fraction pump flow, and systolic/diastolic diameters as previously described (2). Normalized frequency and normalized ejection fraction were derived from internally normalizing frequency and ejection fraction to their respective values in APSS at each respective pressure.

Immunohistochemistry and RNA/Tissue Collection

Rats that were utilized for IHC were euthanized and the mesenteric tissue from the duodenum to the cecum was immediately collected. The ileum was excised and pinned out in a sylgard-coated dish for immunofluorescence. The ileum tissues were then fixed in methanol at −20°C for 1hr. Methanol fixed tissue was rinsed with PBS and the perivascular tissue was cut from the intestinal wall and root of the mesentery, such that two neurovascular bundles were present in each section. These tissues were then transferred to a clean dish and blocked with 5% goat serum in PBS for 2 hours at room temperature. The tissue was then stained overnight at 4°C with antibodies recognizing CD163 at 1:200 (AbD Serotec, MCA342GA), CD206 at1:100 (Abcam, ab64693), and MHCII at 1:200 (Santa Cruz, sc-53721) in combination. Tissues were then washed with PBS and stained with

Author Manuscript Author Manuscript Author Manuscript Author Manuscript

AlexaFlour® 488 or 647-conjugated goat secondary antibodies at 1:200 for the respective primary antibody host and isotype. Tissues were then mounted between two coverslips with Anti-fade® mounting solution to limit the restriction in tissue depth. Images were collected at 20× and 40× magnifications using a Leica scanning confocal microscope with lymphatic vessels centered in the field of view with stacks averaging 50μm at 1μm per slice. One to three lymphatic vessels were imaged from the intestinal wall towards the root of the mesentery per staining combination. Cell counts from five separate 40× images and three separate 20× images were averaged per animal to get an accurate representation of tissue macrophage polarization and lymphatic vessel association. Maximum intensity projections were obtained using FIJI, despeckled, and the projections overlayed. Single positive or double positive cells were counted. The FIJI program COLOC2 was also used to assist in the analysis to confirm co-localization and background subtraction algorithm was utilized for better visualization.

The remaining mesenteric tissues, jejunum to the ileum, were also pinned out and fixed in RNALater ® overnight at 4°C for RNA isolation. The tissue was homogenized in Trizol® *(Life Technologies) the homogenate was then centrifuged for one minute at 1,000g and the lipid content removed to prevent interference in the RNA collection. RNA was then extracted as per the manufacturer's instruction and then further purified with the GenElute ® Mammalian Total RNA kit (Sigma). Additionally, the cecum of each six control and MetSyn rats were cleared of adipose tissue, dabbed dry, and ultimately weighed and measured.

Lymphatic Endothelial Cell and Muscle cell Cultures

Mesenteric lymphatic endothelial cells (LECs) and mesenteric lymphatic muscle cells (LMCs) were both obtained through mesenteric vessel explants. Cells were grown in EGM-2MV medium (Lonza) and used at passages 4–7. LECs were plated at a 60% confluence in a 12-well plate and allowed to grow to a 100% confluence. The LECs were then serum starved with basal EGM media for 2 hours and exposed to either EGM-2MV supplemented with vehicle or LPS (20ng/ml) for 24 hours. These LECs were then washed with ice-cold PBS and lysed in Trizol Reagent® (Life Sciences). RNA was collected as per the manufacturer's instructions. The LMCs were plated at approximately 50% confluence and grown in Dulbecco's modified Eagle's medium (DMEM) with 10% fetal bovine serum (FBS). Upon reaching 80% confluence the LMCs were serum starved for 2 hours in basal DMEM. The media was then replaced with DMEM supplemented with 2% serum and either PBS vehicle or LPS (20ng/ml) for 24 hours. Finally, the LMCs were then washed with ice-cold PBS and RNA collected as described above.

Quantitative Polymerase Chain Reaction (QPCR) Analysis

1 μg of RNA from the tissues, LECs, and LMCs was converted to cDNA using the Bio-Rad iScript cDNA Synthesis Kit®. Gene expression was analyzed using the ΔΔCt method with beta-actin and smooth muscle alpha actin as housekeeping control genes in LECs and LMCs respectively. Beta-actin was also used for internal housekeeping control in the neurovascular bundles tissue QPCR. Primers: β-Actin forward AAGTCCCTCACCCTCCCAAAAG, reverse AAGCAATGCTGTCACCTTCCC; SM α-Actin forward CATCAGGAAGGACCTCTATGC, reverse CTGATCCACATCTGCTGGAAG, interleukin

Author Manuscript Author Manuscript Author Manuscript Author Manuscript

six (IL-6) forward TCCTACCCCAACTTCCAATGCTC, reverse TTGGATGGTCTTGGTCCTTAGCC; CCL2 forward AGCATCCACGTGCTGTCTC, reverse GATCATCTTGCCAGTGAATGAG; iNOS forward CAGCCCTCAGAGTACAACGAT, reverse CAGCAGGCACACGCAATGAT; MCSF forward CCATCGAGACCCTCGGACAT, reverse TGTGTGCCCAGCTTAGAATC; GMCSF forward GACCATGATAGCCAGCCACT, reverse TTCCAGCAGTCAAAAGGGATA; c-c chemokine ligand 1 CCL1 forward GAAGGTGAAGCCCTGCTAAT, reverse GAGAGATGGCTGTGGTTGAG; tumor growth factor-beta (TGFβ) forward CGTGGAAATCAATGGGATCAG, reverse GGAAGGGTCGGTTCATGTCA; macrophage migration inhibitory factor (MIF) forward TGCCAGAGGGGTTTCTCTC, reverse CGCTCGTGCCACTAAAAGTC.

Statistics

Cecum to body weight ratios results were analyzed with a two-tailed Student's T-Test. Macrophage counts and rmLEC/rmLMC QPCR were determined with ANOVA. Statistical significance of isobaric contractile parameters were determined through two-way analysis of variance with Fisher's post hoc analysis using the Statplus® (AnalystSoft) statistical software package. Data are represented as means ± standard error (SE) and significance represented independently at each figure.

Results

Gross Histological Alterations in the Cecum and Perivascular Adipose in MetSyn Rats

Cecums were collected from both MetSyn and control rats after a pre-operative fasting period; the cecum from MetSyn group was smaller in width and length, and in weight when compared to the cecum from control rats (Figure 1A–C). As we have previously reported (79), there was expansion of the perivascular adipose tissue in the MetSyn neurovascular bundles that was further evident after fixation with RNALater® overnight at 4°C (Figures 1D). RNA was extracted from these mesenteric neurovascular bundles and we found a significant increase in the expression of c-c chemokine ligand 2 (also known as monocyte chemoattractant protein 1, CCL2) and the inducible nitric oxide synthase (Figure 1E). As previously reported, we did not observe any significant change in body mass over the seven-week diet period (data not shown).

High-Fructose-Induced MetSyn Rats Exhibited Macrophages Skewed Toward M1 State

We preformed dual staining immunofluorescence on fixed mesenteric arcades with CD11b, CD163, macrophage mannose receptor (CD206), and major histocompatibility complex II (MHCII) expression to delineate macrophage investiture into the mesenteric tissue and lymphatic collecting vessels. Cd11b is a common macrophage marker in the mouse, but very few rat macrophages were positive for CD11b+ in either control or MetSyn tissues (Figure 2 A, E). In control rats, there was an apparent dichotomy in the staining of macrophages with the majority positive for CD163 and CD206, but negative for MHCII ($CD163^{+}CD206^{+}MHCII^{-}$) and a second population of $CD163^{-}CD206^{-}MHCII^{+}$ cells as previously described (9) (Figures 2A–D). The double positive $CD163^{+}CD206^{+}MHCII^{-}$ macrophages (Figures 2D and H) demonstrate the classic "L" shape morphology and

Author Manuscript Author Manuscript Author Manuscript Author Manuscript

staining profile as prototypical adipose tissue macrophages. $CD163^{+}CD206^{+}MHCII^{-}$ were observed both within the clear field mesenteric sheath, throughout the perivascular adipose tissue, and also associated with the lymphatic vasculature (Figures 2D and H). In both control (Figures 2 B and C; red label) and MetSyn rats (Figures 2 F and G; red label), the $CD163^{-}CD206^{-}MHCII^{+}$ macrophage subset is the minor population of the total cells (approximately 30.3% and 34.6% per FOV in control and MetSyn tissues, respectively) and they display a significant tropism towards both lymphatic and blood vasculature structures. The $CD163^{-}CD206^{-}MHCII^{+}$ macrophages often had multiple cell extensions and often were elongated in parallel with the associated vascular structure similar to previous reports (5, 9). There was a significant increase in the population of $CD163^{+}CD206^{+}MHCII^{+}$ cells observed in MetSyn arcades (Figures 2L, M and N). In control rats $CD163^{+}CD206^{+}MHCII^{+}$ cells made up only 6.5% of the total cells per field of view (Figures 2I, K and J), but more than doubled to 14.4% of total cells in the MetSyn tissue. There was no difference in the spatial distribution ratios of the $CD163^{+}CD206^{+}MHCII^{+}$ cells within the MetSyn tissue as compared to controls, as similar ratios in the tissue space and in contact with the vessel were not significantly different. MetSyn mesenteric bundles also had a significant increase in the total number of macrophages per field of view (Figure 2O) and the increased presence of the $CD163^{+}CD206^{+}MHCII^{+}$ macrophages can account for this difference (Figure 2P). There were no significant changes observed in the population of $CD163^{+}CD206^{+}MHCII^{-}$ nor $CD163^{-}CD206^{-}MHCII^{+}$ macrophages in MetSyn arcades (data not shown).

Macrophage Recruitment and Polarization Factors by Lymphatic Tissue

To address whether in response to inflammation, the lymphatic cells produce conducible environment for macrophage recruitment, cultured LECs and LMCs from tissue explants were treated with 20ng/ml of LPS for a 24-hour period. We found that LECs significantly up-regulated the expression of MIF, MCSF, IL-6, and TNFα in response to LPS stimulation (Figures 3A and B). However, the largest expression changes were observed in iNOS, CCL1, CCL2, and GMCSF expression in LECs, which all were substantially up regulated in response to LPS (Figure 3A). MCSF, but not GMCSF, expression was readily detected in untreated LECs and there was a significant increase in expression of MCSF in response to LPS. LEC GMCSF expression had the highest up regulation of the genes tested in response to LPS (Figure 3B). LMCs did not display the differential regulation of MCSF and GMCSF as both genes were up regulated along with TGFβ in response to LPS (Figures 3C and D). As in LECs, both iNOS and CCL2 expression were significantly up regulated in LMC in addition to IL-6.

Partial Improvement in MLV contractility with LNAME and Glib

We have previously reported that the lymphatic collecting vessel contractility is diminished in the MetSyn phenotype (79). We observed similar impairments in the contraction frequency and lymphatic pump output in MetSyn MLVs consistent with previous reports (Figures 4A–D). Since excessive NO exposure is known to inhibit lymphatic contractility, we tested whether inhibition of NO would improve the lymphatic function in the MetSyn group. Representative traces at P=3cm in APSS and 100μm LNAME are shown for lymphatics isolated from control and MetSyn rats (Figure 5A). Control MLVs treated with 100μm LNAME did not demonstrate any significant difference in contraction frequency,

Author Manuscript Author Manuscript Author Manuscript Author Manuscript

ejection fraction, fractional pump flow, or vessel tone changes. In contrast, lymphatics from MetSyn rats treated with LNAME resulted in a significant, increase in contraction frequency at pressures 1cm and 3cmH_2O (Figures 5B and C). The elevation in contraction frequency was able to significantly increase MetSyn MLV FPF at pressures of 1cm and 3cmH_2O (Figure 5D).

Mesenteric lymphatic collecting vessel contraction frequency is dependent on resting membrane potential. Activation of the ATP sensitive potassium channels (K_{ATP}) lead to membrane hyperpolarization and reduction in contraction frequency. We used the K_{ATP} inhibitor, and anti-diabetic drug, glibenclamide to inhibit the endogenous K_{ATP} channels at 1μm and 10μm and restore lymphatic contractility (Figure 6A). Control MLVs contraction frequency, ejection fraction, and fractional pump flow were not statistically different in response to 1μM Glib. MetSyn contraction frequency and fractional pump flow (Figures 6B and 6D) were significantly increased at P=1 cmH_2O, but neither at P=3cm or at 7 cmH_2O after stimulation with 1μM Glib. We also employed Glib at 10μM and this resulted in a significant activation of contraction frequency in both control and MetSyn vessels (Figure 6B). Such robust activation of contraction frequency diminished the filling period, and reduced ejection fraction (Figure 6C). As a result, 10μM Glib did not significantly affect fractional pump flow in control vessels. In contrast fractional pump flow was significantly increased at pressures of 1cm and 3cmH_2O in MetSyn vessels with 10μM Glib. A total list of lymphatic contractile parameters is given in Table 1.

Discussion

The presented data demonstrate that MLV contractility impairment is associated with increased macrophage investiture into, and along, the mesenteric lymphatic collecting vessels after induction of MetSyn with high fructose feeding. In addition to the $CD163^+CD206^+MHCII^-$ and $CD163^-CD206^-MHCII^+$ macrophage populations observed in control rats, the MetSyn rats had significant increase in the $CD163^+CD206^+MHCII^+$ macrophages both within the perivascular tissue and in association with the lymphatic vasculature. $CD163^+CD206^+MHCII^+$ likely represent the inflammatory M1 skewed polarization that is often observed in canonical adipose depots of obese and diabetic rodent models (44). We also demonstrate a role for the lymphatic tissue itself, both endothelium and muscle cells, as a mechanism for chemotactic stimulus, CCL2, as well as cytokines that influence macrophage polarization by exposure to the common dietary endotoxin LPS. The dysfunction in MetSyn MLV contractility was partially ameliorated by inhibition of NOS activity with LNAME and the K_{ATP} channel inhibitor Glib.

We observed an increase in the perivascular adiposity of the mesenteric neurovascular bundles in the MetSyn rats supporting our previously finding (79). Interestingly, we consistently observed smaller cecum in the MetSyn cohort. The change in fasted cecum weight and size could be attributed to the ease by which fructose can be absorbed as a monosaccharide. It is also important to note that the high fructose feed model induces hyper formation of chylomicrons within the enterocytes of the intestine (16, 27). The chylomicron formation process results in the absorption of bacterial components, luminal antigens (72), and particularly LPS (25), which account for the metabolic endotoxemia and source of

Author Manuscript Author Manuscript Author Manuscript Author Manuscript

inflammation reported in most models of metabolic disease (7, 13, 57). Chylomicrons and their associated LPS are then released into the lamina propria, up taken by the lymphatic capillaries, and ultimately pass through the mesenteric lymphatic collecting vessels studied in this work. Although elevated endotoxins and TLR activity have been well documented in metabolic diseases (17, 29, 67), we did not assess lymph or blood LPS levels in the control nor MetSyn rats and cannot directly link the LPS or other endotoxins as the causative agent for the lymphatic dysfunction we observed in MetSyn rats.

Expansion of adipose tissue is now fundamentally linked with alterations in the immunological fingerprint of adipose tissues. Of particular significance is the increased accumulation of macrophages (73) that are polarized toward the classical inflammatory M1 phenotype (44). Our data provides the first characterization of the M1 skewed macrophage polarization and the spatial association with lymphatic collecting vessels in MetSyn rats. Control rats demonstrated two major macrophage populations within the mesenteric tissue that could be delineated with our staining profile into $CD163^{+}CD206^{+}MHCII^{-}$ and $CD163^{-}CD206^{-}MHCII^{+}$. We observed minor populations of both $CD206^{+}/CD163^{+}CD11b^{+}$ and $MHCII^{+}CD11b^{+}$ cells under both control and MetSyn conditions suggesting an intermediate cell phenotype before they polarize into the dominant phenotypes that appear to be CD11b negative. The $CD163^{+}CD206^{+}MHCII^{-}$ bare similarity to the canonical adipose M2 macrophages and are found throughout the perivascular adipose tissue but also distributed across the mesothelial sheath that encloses the tissue space. The $CD163^{-}CD206^{-}MHCII^{+}$ macrophages display significant tropism for both blood capillaries and lymphatic vasculature structures. Interestingly, there were no changes in the spatial ratios of $CD163^{+}CD206^{+}MHCII^{+}$ cells in the MetSyn tissue. The $CD163^{+}CD206^{+}MHCII^{-}$ cells are evenly distributed throughout the tissue and the $CD163^{-}CD206^{-}MHCII^{+}$ cells are predominantly found on the vascular structures. We interpret this as that multiple chemokine signaling pathways must exist within the lymphatic tissue to promote the association of multiple immune cell populations. Induction of MetSyn increased the total macrophage investiture within the neurovascular bundle. Neither the $CD163^{+}CD206^{+}MHCII^{-}$ nor the $CD163^{-}CD206^{-}MHCII^{+}$ phenotypes were significantly affected by MetSyn. Instead we found a significant increase in $CD163^{+}CD206^{+}MHCII^{+}$ macrophages that was the basis for increased macrophage accumulation and that we have interpreted as M1 skewed adipose tissue macrophage (44). The robust hyperglycemia and hyperinsulinemia observed in the high fructose model fit well with the observed inflammation and macrophage shift. M1 macrophages play a critical role in the insulin desensitization and adipose dysfunction in metabolic syndrome models through the production of inflammatory signaling molecules such as IL-6, TNFα, and IL-1β (30, 67, 77).

Recent reports have suggested that macrophage polarization resembles a spectrum as opposed to specific phenotypes (51). In addition to potent signaling molecules such as IL-4, IL-13, and IFNγ, macrophage polarization can be skewed through the concentration ratio of MCSF and GMCSF into M2 or M1 macrophages respectively (32). Specifically, GMCSF promotes the M1 phenotype as evident by expression of MHCII, increased co-stimulatory molecule expression, and inflammatory cytokine production (22, 37). Both MCSF and GMCSF are expressed in multiple cell types and likely provide the regional cues for macrophage activation prior to robust T cell activation. In this study we have demonstrated

Author Manuscript Author Manuscript Author Manuscript Author Manuscript

that both LMCs and LECs contribute to the MCSF and GMCSF expression basally and in response to LPS stimulation. Given the lymphatic role in antigen presenting cell (APC) recruitment, direct exposure to lymph, and spatial association with macrophages phenotypes within the tissue suggest a dominant stromal function for LECs and LMCs. Of particular significance was the expression relationship of MCSF and GMCSF within the LECs in response to LPS. LECs expressed high levels of MCSF and CCL2 basally while GMCSF was almost below detectable levels. However, after stimulation with LPS LECs dramatically increased GMCSF beyond MCSF expression levels and further increased CCL2 expression despite only mild up-regulation of MCSF. Thus the LECs act as a molecular switch that can alter both the tissue MCSF/GMCSF ratio but also condition the lymph and thereby affect the cell populations within the node. MCSF and GMCSF regulation by lymphatic tissues has direct bearing on myeloid recruitment and differentiation (28, 32, 37), regional inflammation (34), cancer progression (38, 58), and lymphangiogenesis (36). Previous studies have demonstrated that the lymphatic endothelium expresses TLRs and is sensitive to most TLR agonists (33, 56). Infection of LECs with cytomegalovirus also increases the production of GMCSF (21) and GM-CSF levels in lymph are elevated during inflammation. Dietary endotoxin is a significant contributor to the inflammation in the adipose tissue and liver, and GMCSF expression has been linked to adipose inflammation and insulin resistance (6, 7, 34). Thus our data demonstrate that lymphatic tissues have the potential to contribute to macrophage recruitment and inflammation in MetSyn. The LECs and LMCs utilized in this study were from primary explant cultures of normal mesenteric lymphatic collecting vessels. MetSyn is characterized by alterations in glucose, lipid, and cytokine levels that each could potentially affect both the baseline expression of these genes and also their regulation in response to TLR stimulus. Hence further in vivo experiments are warranted to determine the mechanisms linking macrophage status (M1 or M2) and lymphatic dysfunction.

We have previously reported that MLV have poor lymphatic function in a high fructose fed rat model of MetSyn as a result of significantly reduced contraction frequency (79). Other investigators have replicated these results in genetic and diet-induced models of obesity and the MetSyn state in the mouse(3, 61, 74). We provide further evidence to support the inclusion of lymphatic dysfunction with microvascular abnormalities as a hallmark of metabolic disease. Consistent with our previous findings (79), MetSyn lymphatic vessels exhibited smaller in size, but no change in tone and lymphatic contractility indexes were significantly reduced in MetSyn rats. Lymphatic vessels are also self-regulating through the generation of NO in response to the shear stress of lymph propulsion (4, 24). Shear-induced NO will activate both PKA and PKG in the smooth muscle that increases adenosine triphosphate (ATP) sensitive potassium channel (K_{ATP}) channel activity, hyperpolarizing the pacemaker and reducing the contraction frequency. In contrast, increased frequency but not ejection fraction in MetSyn animals was insufficient to increase fractional pump flow. Mesenteric lymph pump flow inhibition has been described in other models of chronic inflammation. TNBS-induced ileitis caused significant inhibition of MLV pump in guinea pigs that was restored by the K_{ATP} channel blocker Glib (48, 76). We also assessed the ability of the Glib to increase the lymph pump flow in MetSyn rats. While 1μM Glib had little effect on control MLV contractility, in MetSyn vessels, contraction frequency and fractional pump flow were significantly increased at only the low pressure in response to

Author Manuscript Author Manuscript Author Manuscript Author Manuscript

1μM. However 10μM Glib significantly increased contraction frequency at each pressure in both control and MetSyn rats. This suggests that the MLV pacemaker machinery is intact as observed by maximal stimulation via Glib and that inhibition of MLV contraction frequency in MetSyn is mediated by membrane hyperpolarization.

The effect of LNAME suggest that excessive NO production does not account for the entire lymphatic contractile impairment in MetSyn. Our data showed an increase in iNOS expression in the mesenteric arcades from MetSyn rats (Figure 1E) and a higher level of iNOS expression in LPS-treated LMCs and LECs (Figure 3) indicate that NO availability in the mesenteric bed would have increased in the MetSyn rats. However the source of NO from the macrophages recruited under MetSyn condition must be further investigated. We have recently shown that an increase in the population of monocytes and macrophages in LPS-treated rats establish a robust M2 phenotype with higher expression of CD163 and CD206 (9). The recruitment and association of macrophages with lymphatic tissues have been previously documented with LPS-induced inflammation in a mouse model, although macrophage polarization has not been addressed in these studies (35, 41, 42). A mouse model of LPS-induced peritonitis demonstrated a role for $CD11b^+$ myeloid cells in lymphatic dysfunction and poor fluid clearance in the diaphragm (35). Others have demonstrated a role for iNOS-expressing $CD11b^+$ $Gr1^+$ monocytes in the suppression of mouse popliteal lymphatic contractility in response to oxazolone-driven inflammation (41). In the mouse, iNOS expression strongly correlates with the either the M1 or M2b polarization (44, 46, 51). Extensive studies with the full host of rat macrophage polarization spectrum have yet to be been done to confirm this iNOS paradigm. Intriguingly, iNOS expression and nitric oxide production in human macrophages is limited and controversial (55, 65, 66) suggesting this mechanism may be irrelevant in human lymphedema patients. Furthermore rat peritoneal macrophages have high levels of NO production that is also strain-dependent and may not be limited to specific polarizations and different contractile responses in response to inflammation may be strain dependent (40, 52).

A critical limitation to this study was the inability to directly link iNOS expression to the increased $CD163^+CD206^+MHCII^+$ macrophage population found in the MetSyn rats. Additionally, LNAME is a pan NOS inhibitor and we did not assess the expression or protein levels of NOS1, NOS2, or NOS3 within the vessels themselves. It is possible that cells within the lymphatic wall that express either nNOS or eNOS may also contribute to the inhibition of lymphatic contractile activity. Investigations into the expression of iNOS in the rat macrophage populations will be critical to determining further roles for macrophage polarization function and coordination of lymphatic function.

In conclusion, as summarized in figure 7 the results presented in this study have provided new evidence linking alterations in macrophage activation and polarization with direct and controlled measures of lymphatic vessel contractility under acute and chronic inflammatory conditions. Data have also demonstrated a stromal function for LECs and LMCs in the regulation of macrophage homeostasis through the production of MCSF, GMCSF, and CCL2. Lymphatic dysfunction was apparent despite a lack of gross obesity in MetSyn group. An increase in perivascular adipose expansion has been observed in MetSyn animals that are associated with macrophage polarization skewed to a M1 phenotype. Hence, the

Author Manuscript Author Manuscript Author Manuscript Author Manuscript

data presented here further supports the notion of immunogenic regulation of lymphatic vessel contractility and suggest that the functional characteristics of lymphatics may contribute to resident tissue macrophage homeostasis under physiological and pathophysiological conditions, such as MetSyn, and may contribute to the increased risk for lymphedema in MetSyn.

Perspectives

Lymphatic collecting vessel dysfunction is likely a contributor to poor lymphatic circulation observed in metabolically disturbed patients. Inflammation concurrent with the metabolic syndrome can result in the accumulation of inflammatory cells not only within the tissue, but also along the lymphatic collecting vessels and lymphatic vasculature. Production of inflammatory molecules by the cells in the tissue and along the lymphatic collecting vessel can impair the pump function of these vessels and limit the return of fluid back to the blood circulation and promote tissue edema in MetSyn and other metabolic disorders.

Acknowledgments

This work was supported by NIH RO1 DK99221 to MM and DZ.

References

1. Ahmed RL, Schmitz KH, Prizment AE, Folsom AR. Risk factors for lymphedema in breast cancer survivors, the Iowa Women's Health Study. Breast Cancer Res Treat. 2011
2. Benoit JN, Zawieja DC, Goodman AH, Granger HJ. Characterization of intact mesenteric lymphatic pump and its responsiveness to acute edemagenic stress. Am J Physiol. 1989; 257:H2059–2069. [PubMed: 2603989]
3. Blum KS, Karaman S, Proulx ST, Ochsenbein AM, Luciani P, Leroux JC, Wolfrum C, Detmar M. Chronic high-fat diet impairs collecting lymphatic vessel function in mice. PLoS One. 2014; 9:e94713. [PubMed: 24714646]
4. Bohlen HG, Gasheva OY, Zawieja DC. Nitric oxide formation by lymphatic bulb and valves is a major regulatory component of lymphatic pumping. Am J Physiol Heart Circ Physiol. 2011; 301:H1897–1906. [PubMed: 21890688]
5. Bridenbaugh EA, Wang W, Srimushnam M, Cromer WE, Zawieja SD, Schmidt SE, Jupiter DC, Huang HC, Van Buren V, Zawieja DC. An immunological fingerprint differentiates muscular lymphatics from arteries and veins. Lymphat Res Biol. 2013; 11:155–171. [PubMed: 24044756]
6. Cani PD, Amar J, Iglesias MA, Poggi M, Knauf C, Bastelica D, Neyrinck AM, Fava F, Tuohy KM, Chabo C, Waget A, Delmee E, Cousin B, Sulpice T, Chamontin B, Ferrieres J, Tanti JF, Gibson GR, Casteilla L, Delzenne NM, Alessi MC, Burcelin R. Metabolic endotoxemia initiates obesity and insulin resistance. Diabetes. 2007; 56:1761–1772. [PubMed: 17456850]
7. Cani PD, Bibiloni R, Knauf C, Waget A, Neyrinck AM, Delzenne NM, Burcelin R. Changes in gut microbiota control metabolic endotoxemia-induced inflammation in high-fat diet-induced obesity and diabetes in mice. Diabetes. 2008; 57:1470–1481. [PubMed: 18305141]
8. Chakraborty S, Davis MJ, Muthuchamy M. Emerging trends in the pathophysiology of lymphatic contractile function. Semin Cell Dev Biol. 2015; 38:55–66. [PubMed: 25617600]
9. Chakraborty S, Zawieja SD, Wang W, Lee Y, Wang YJ, von der Weid PY, Zawieja DC, Muthuchamy M. Lipopolysaccharide modulates neutrophil recruitment and macrophage polarization on lymphatic vessels and impairs lymphatic function in rat mesentery. Am J Physiol Heart Circ Physiol. 2015 ajpheart 00467 02015.
10. Cinti S, Mitchell G, Barbatelli G, Murano I, Ceresi E, Faloia E, Wang S, Fortier M, Greenberg AS, Obin MS. Adipocyte death defines macrophage localization and function in adipose tissue of obese mice and humans. J Lipid Res. 2005; 46:2347–2355. [PubMed: 16150820]

Author Manuscript Author Manuscript Author Manuscript Author Manuscript

11. Davis MJ, Zawieja DC, Gashev AA. Automated measurement of diameter and contraction waves of cannulated lymphatic microvessels. Lymphat Res Biol. 2006; 4:3–10. [PubMed: 16569200]
12. Dean SM, Zirwas MJ, Horst AV. Elephantiasis nostras verrucosa: an institutional analysis of 21 cases. J Am Acad Dermatol. 2011; 64:1104–1110. [PubMed: 21440328]
13. Dogan S, Celikbilek M, Guven K. High fructose consumption can induce endotoxemia. Gastroenterology. 2012; 143:e29. author reply e29.
14. Engeset A, Olszewski W, Jaeger PM, Sokolowski J, Theodorsen L. Twenty-four hour variation in flow and composition of leg lymph in normal men. Acta physiologica Scandinavica. 1977; 99:140–148. [PubMed: 842370]
15. Farshid G, Weiss SW. Massive localized lymphedema in the morbidly obese: a histologically distinct reactive lesion simulating liposarcoma. The American journal of surgical pathology. 1998; 22:1277–1283. [PubMed: 9777990]
16. Federico LM, Naples M, Taylor D, Adeli K. Intestinal insulin resistance and aberrant production of apolipoprotein B48 lipoproteins in an animal model of insulin resistance and metabolic dyslipidemia: evidence for activation of protein tyrosine phosphatase-1B, extracellular signal-related kinase, and sterol regulatory element-binding protein-1c in the fructose-fed hamster intestine. Diabetes. 2006; 55:1316–1326. [PubMed: 16644688]
17. Festi D, Schiumerini R, Eusebi LH, Marasco G, Taddia M, Colecchia A. Gut microbiota and metabolic syndrome. World J Gastroenterol. 2014; 20:16079–16094. [PubMed: 25473159]
18. Fife C. Massive localized lymphedema, a disease unique to the morbidly obese: a case study. Ostomy Wound Manage. 2014; 60:30–35.
19. Fife CE, Benavides S, Carter MJ. A patient-centered approach to treatment of morbid obesity and lower extremity complications: an overview and case studies. Ostomy Wound Manage. 2008; 54:20–22. [PubMed: 18250484]
20. Fife CE, Carter MJ. Lymphedema in the morbidly obese patient: unique challenges in a unique population. Ostomy Wound Manage. 2008; 54:44–56.
21. Fiorentini S, Luganini A, Dell'Oste V, Lorusso B, Cervi E, Caccuri F, Bonardelli S, Landolfo S, Caruso A, Gribaudo G. Human cytomegalovirus productively infects lymphatic endothelial cells and induces a secretome that promotes angiogenesis and lymphangiogenesis through interleukin-6 and granulocyte-macrophage colony-stimulating factor. The Journal of general virology. 2011; 92:650–660. [PubMed: 21123547]
22. Fleetwood AJ, Lawrence T, Hamilton JA, Cook AD. Granulocyte-macrophage colony-stimulating factor (CSF) and macrophage CSF-dependent macrophage phenotypes display differences in cytokine profiles and transcription factor activities: implications for CSF blockade in inflammation. J Immunol. 2007; 178:5245–5252. [PubMed: 17404308]
23. Gashev AA, Davis MJ, Zawieja DC. Inhibition of the active lymph pump by flow in rat mesenteric lymphatics and thoracic duct. J Physiol. 2002; 540:1023–1037. [PubMed: 11986387]
24. Gasheva OY, Zawieja DC, Gashev AA. Contraction-initiated NO-dependent lymphatic relaxation: a self-regulatory mechanism in rat thoracic duct. J Physiol. 2006; 575:821–832. [PubMed: 16809357]
25. Ghoshal S, Witta J, Zhong J, de Villiers W, Eckhardt E. Chylomicrons promote intestinal absorption of lipopolysaccharides. J Lipid Res. 2009; 50:90–97. [PubMed: 18815435]
26. Grundy SM. Obesity, metabolic syndrome, and cardiovascular disease. J Clin Endocrinol Metab. 2004; 89:2595–2600. [PubMed: 15181029]
27. Haidari M, Leung N, Mahbub F, Uffelman KD, Kohen-Avramoglu R, Lewis GF, Adeli K. Fasting and postprandial overproduction of intestinally derived lipoproteins in an animal model of insulin resistance. Evidence that chronic fructose feeding in the hamster is accompanied by enhanced intestinal de novo lipogenesis and ApoB48-containing lipoprotein overproduction. J Biol Chem. 2002; 277:31646–31655. [PubMed: 12070142]
28. He H, Xu J, Warren CM, Duan D, Li X, Wu L, Iruela-Arispe ML. Endothelial cells provide an instructive niche for the differentiation and functional polarization of M2-like macrophages. Blood. 2012; 120:3152–3162. [PubMed: 22919031]
29. Himes RW, Smith CW. Tlr2 is critical for diet-induced metabolic syndrome in a murine model. FASEB J. 2010; 24:731–739. [PubMed: 19841034]

Author Manuscript Author Manuscript Author Manuscript Author Manuscript

30. Hotamisligil GS, Shargill NS, Spiegelman BM. Adipose expression of tumor necrosis factor-alpha: direct role in obesity-linked insulin resistance. Science. 1993; 259:87–91. [PubMed: 7678183]
31. Huxley VH, Scallan J. Lymphatic fluid: exchange mechanisms and regulation. J Physiol. 2011; 589:2935–2943. [PubMed: 21521763]
32. Jaguin M, Houlbert N, Fardel O, Lecureur V. Polarization profiles of human M-CSF-generated macrophages and comparison of M1-markers in classically activated macrophages from GM-CSF and M-CSF origin. Cellular immunology. 2013; 281:51–61. [PubMed: 23454681]
33. Kang S, Lee SP, Kim KE, Kim HZ, Memet S, Koh GY. Toll-like receptor 4 in lymphatic endothelial cells contributes to LPS-induced lymphangiogenesis by chemotactic recruitment of macrophages. Blood. 2009; 113:2605–2613. [PubMed: 19098273]
34. Kim DH, Sandoval D, Reed JA, Matter EK, Tolod EG, Woods SC, Seeley RJ. The role of GM-CSF in adipose tissue inflammation. Am J Physiol Endocrinol Metab. 2008; 295:E1038–1046. [PubMed: 18765677]
35. Kim KE, Koh YJ, Jeon BH, Jang C, Han J, Kataru RP, Schwendener RA, Kim JM, Koh GY. Role of CD11b+ macrophages in intraperitoneal lipopolysaccharide-induced aberrant lymphangiogenesis and lymphatic function in the diaphragm. Am J Pathol. 2009; 175:1733–1745. [PubMed: 19762711]
36. Kubota Y, Takubo K, Shimizu T, Ohno H, Kishi K, Shibuya M, Saya H, Suda T. M-CSF inhibition selectively targets pathological angiogenesis and lymphangiogenesis. J Exp Med. 2009; 206:1089–1102. [PubMed: 19398755]
37. Lacey DC, Achuthan A, Fleetwood AJ, Dinh H, Roiniotis J, Scholz GM, Chang MW, Beckman SK, Cook AD, Hamilton JA. Defining GM-CSF- and macrophage-CSF-dependent macrophage responses by in vitro models. J Immunol. 2012; 188:5752–5765. [PubMed: 22547697]
38. Laoui D, Van Overmeire E, De Baetselier P, Van Ginderachter JA, Raes G. Functional Relationship between Tumor-Associated Macrophages and Macrophage Colony-Stimulating Factor as Contributors to Cancer Progression. Frontiers in immunology. 2014; 5:489. [PubMed: 25339957]
39. Lee S, Roizes S, von der Weid PY. Distinct roles of L- and T-type voltage-dependent Ca2+ channels in regulation of lymphatic vessel contractile activity. J Physiol. 2014; 592:5409–5427. [PubMed: 25326448]
40. Li Z, Zhao ZJ, Zhu XQ, Ren QS, Nie FF, Gao JM, Gao XJ, Yang TB, Zhou WL, Shen JL, Wang Y, Lu FL, Chen XG, Hide G, Ayala FJ, Lun ZR. Differences in iNOS and arginase expression and activity in the macrophages of rats are responsible for the resistance against T. gondii infection. PLoS One. 2012; 7:e35834. [PubMed: 22558235]
41. Liao S, Cheng G, Conner DA, Huang Y, Kucherlapati RS, Munn LL, Ruddle NH, Jain RK, Fukumura D, Padera TP. Impaired lymphatic contraction associated with immunosuppression. Proceedings of the National Academy of Sciences of the United States of America. 2011; 108:18784–18789. [PubMed: 22065738]
42. Lobov GI, Kubyshkina NA. Mechanisms underlying the effect of E. coli endotoxin on contractile function of lymphatic vessels. Bull Exp Biol Med. 2004; 137:114–116. [PubMed: 15273751]
43. Loughlin V. Massive obesity simulating lymphedema. N Engl J Med. 1993; 328:1496.
44. Lumeng CN, Bodzin JL, Saltiel AR. Obesity induces a phenotypic switch in adipose tissue macrophage polarization. J Clin Invest. 2007; 117:175–184. [PubMed: 17200717]
45. Lumeng CN, DelProposto JB, Westcott DJ, Saltiel AR. Phenotypic switching of adipose tissue macrophages with obesity is generated by spatiotemporal differences in macrophage subtypes. Diabetes. 2008; 57:3239–3246. [PubMed: 18829989]
46. Mantovani A, Sica A, Sozzani S, Allavena P, Vecchi A, Locati M. The chemokine system in diverse forms of macrophage activation and polarization. Trends Immunol. 2004; 25:677–686. [PubMed: 15530839]
47. Marken Lichtenbelt WD, Fogelholm M. Increased extracellular water compartment, relative to intracellular water compartment, after weight reduction. Journal of applied physiology. 1999; 87:294–298. [PubMed: 10409587]
48. Mathias R, von der Weid PY. Involvement of the NO-cGMP-K(ATP) channel pathway in the mesenteric lymphatic pump dysfunction observed in the guinea pig model of TNBS-induced ileitis. Am J Physiol Gastrointest Liver Physiol. 2013; 304:G623–634. [PubMed: 23275612]

Author Manuscript Author Manuscript Author Manuscript Author Manuscript

49. Modolin ML, Cintra W Jr, Paggiaro AO, Faintuch J, Gemperli R, Ferreira MC. Massive localized lymphedema (MLL) in bariatric candidates. Obesity surgery. 2006; 16:1126–1130. [PubMed: 16989693]
50. Modolin ML, Cintra W Jr, Paggiaro AO, Faintuch J, Gemperli R, Ferreira MC. Massive localized lymphedema (MLL) in bariatric candidates. Obes Surg. 2006; 16:1126–1130. [PubMed: 16989693]
51. Mosser DM, Edwards JP. Exploring the full spectrum of macrophage activation. Nat Rev Immunol. 2008; 8:958–969. [PubMed: 19029990]
52. Mullner N, Lazar A, Hrabak A. Enhanced utilization and altered metabolism of arginine in inflammatory macrophages caused by raised nitric oxide synthesis. The international journal of biochemistry & cell biology. 2002; 34:1080–1090. [PubMed: 12009303]
53. Olszewski WL. Contractility patterns of normal and pathologically changed human lymphatics. Ann N Y Acad Sci. 2002; 979:52–63. discussion 76-59. [PubMed: 12543716]
54. Oron-Herman M, Kamari Y, Grossman E, Yeger G, Peleg E, Shabtay Z, Shamiss A, Sharabi Y. Metabolic syndrome: comparison of the two commonly used animal models. Am J Hypertens. 2008; 21:1018–1022. [PubMed: 18566592]
55. Padgett EL, Pruett SB. Evaluation of nitrite production by human monocyte-derived macrophages. Biochemical and biophysical research communications. 1992; 186:775–781. [PubMed: 1497665]
56. Pegu A, Qin S, Fallert Junecko BA, Nisato RE, Pepper MS, Reinhart TA. Human lymphatic endothelial cells express multiple functional TLRs. J Immunol. 2008; 180:3399–3405. [PubMed: 18292566]
57. Pendyala S, Walker JM, Holt PR. A high-fat diet is associated with endotoxemia that originates from the gut. Gastroenterology. 2012; 142:1100–1101 e1102. [PubMed: 22326433]
58. Priceman SJ, Sung JL, Shaposhnik Z, Burton JB, Torres-Collado AX, Moughon DL, Johnson M, Lusis AJ, Cohen DA, Iruela-Arispe ML, Wu L. Targeting distinct tumor-infiltrating myeloid cells by inhibiting CSF-1 receptor: combating tumor evasion of antiangiogenic therapy. Blood. 2010; 115:1461–1471. [PubMed: 20008303]
59. Recek C. Venous pressure gradients in the lower extremity and the hemodynamic consequences. Vasa. 2010; 39:292–297. [PubMed: 21104617]
60. Rockson SG. Causes and consequences of lymphatic disease. Annals of the New York Academy of Sciences. 2010; 1207(Suppl 1):E2–6. [PubMed: 20961302]
61. Savetsky IL, Torrisi JS, Cuzzone DA, Ghanta S, Albano NJ, Gardenier JC, Joseph WJ, Mehrara BJ. Obesity increases inflammation and impairs lymphatic function in a mouse model of lymphedema. Am J Physiol Heart Circ Physiol. 2014; 307:H165–172. [PubMed: 24858842]
62. Scallan JP, Davis MJ. Genetic removal of basal nitric oxide enhances contractile activity in isolated murine collecting lymphatic vessels. J Physiol. 2013; 591:2139–2156. [PubMed: 23420659]
63. Scallan JP, Huxley VH. In vivo determination of collecting lymphatic vessel permeability to albumin: a role for lymphatics in exchange. J Physiol. 2010; 588:243–254. [PubMed: 19917564]
64. Scheinfeld NS. Obesity and dermatology. Clin Dermatol. 2004; 22:303–309. [PubMed: 15475230]
65. Schneemann M, Schoeden G. Macrophage biology and immunology: man is not a mouse. Journal of leukocyte biology. 2007; 81:579. discussion 580. [PubMed: 17332373]
66. Schneemann M, Schoedon G, Hofer S, Blau N, Guerrero L, Schaffner A. Nitric oxide synthase is not a constituent of the antimicrobial armature of human mononuclear phagocytes. The Journal of infectious diseases. 1993; 167:1358–1363. [PubMed: 7684756]
67. Shi H, Kokoeva MV, Inouye K, Tzameli I, Yin H, Flier JS. TLR4 links innate immunity and fatty acid-induced insulin resistance. J Clin Invest. 2006; 116:3015–3025. [PubMed: 17053832]
68. van Rij AM, De Alwis CS, Jiang P, Christie RA, Hill GB, Dutton SJ, Thomson IA. Obesity and impaired venous function. Eur J Vasc Endovasc Surg. 2008; 35:739–744. [PubMed: 18313335]
69. Vasileiou AM, Bull R, Kitou D, Alexiadou K, Garvie NJ, Coppack SW. Oedema in obesity; role of structural lymphatic abnormalities. Int J Obes (Lond). 2011; 35:1247–1250. [PubMed: 21266949]
70. von der Weid PY, Zhao J, Van Helden DF. Nitric oxide decreases pacemaker activity in lymphatic vessels of guinea pig mesentery. Am J Physiol Heart Circ Physiol. 2001; 280:H2707–2716. [PubMed: 11356627]

Author Manuscript Author Manuscript Author Manuscript Author Manuscript

71. Waki M, Kral JG, Mazariegos M, Wang J, Pierson RN Jr, Heymsfield SB. Relative expansion of extracellular fluid in obese vs. nonobese women. The American journal of physiology. 1991; 261:E199–203. [PubMed: 1872382]

72. Wang Y, Ghoshal S, Ward M, de Villiers W, Woodward J, Eckhardt E. Chylomicrons promote intestinal absorption and systemic dissemination of dietary antigen (ovalbumin) in mice. PLoS One. 2009; 4:e8442. [PubMed: 20041190]

73. Weisberg SP, McCann D, Desai M, Rosenbaum M, Leibel RL, Ferrante AW Jr. Obesity is associated with macrophage accumulation in adipose tissue. J Clin Invest. 2003; 112:1796–1808. [PubMed: 14679176]

74. Weitman ES, Aschen SZ, Farias-Eisner G, Albano N, Cuzzone DA, Ghanta S, Zampell JC, Thorek D, Mehrara BJ. Obesity impairs lymphatic fluid transport and dendritic cell migration to lymph nodes. PLoS One. 2013; 8:e70703. [PubMed: 23950984]

75. Wu D, Molofsky AB, Liang HE, Ricardo-Gonzalez RR, Jouihan HA, Bando JK, Chawla A, Locksley RM. Eosinophils sustain adipose alternatively activated macrophages associated with glucose homeostasis. Science. 2011; 332:243–247. [PubMed: 21436399]

76. Wu TF, Carati CJ, Macnaughton WK, von der Weid PY. Contractile activity of lymphatic vessels is altered in the TNBS model of guinea pig ileitis. Am J Physiol Gastrointest Liver Physiol. 2006; 291:G566–574. [PubMed: 16675748]

77. Xu H, Barnes GT, Yang Q, Tan G, Yang D, Chou CJ, Sole J, Nichols A, Ross JS, Tartaglia LA, Chen H. Chronic inflammation in fat plays a crucial role in the development of obesity-related insulin resistance. J Clin Invest. 2003; 112:1821–1830. [PubMed: 14679177]

78. Zawieja DC. Contractile physiology of lymphatics. Lymphat Res Biol. 2009; 7:87–96. [PubMed: 19534632]

79. Zawieja SD, Wang W, Wu X, Nepiyushchikh ZV, Zawieja DC, Muthuchamy M. Impairments in the intrinsic contractility of mesenteric collecting lymphatics in a rat model of metabolic syndrome. Am J Physiol Heart Circ Physiol. 2012; 302:H643–653. [PubMed: 22159997]

Author Manuscript Author Manuscript Author Manuscript Author Manuscript

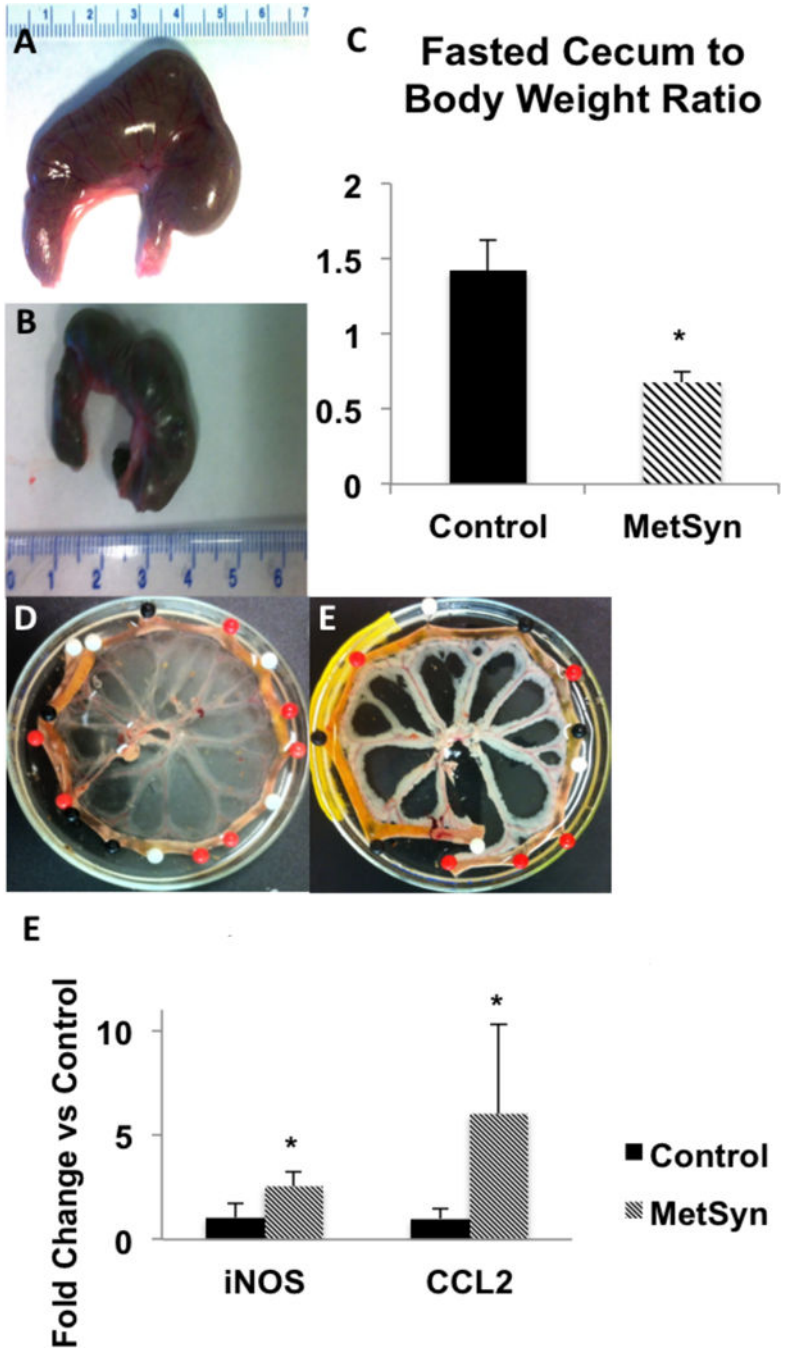

Figure 1.

High fructose feeding-induced MetSyn results in gross histological changes in the cecum and mesenteric tissue. Cecum size in control (A) and MetSyn (B) rats is shown; (C) Cecum weight to body weight is shown for control and MetSyn rats (n=6). Mesenteric tissue bundles fixed in RNALater® overnight at 4°C illuminates the increased adiposity in the perivascular depots of the mesenteric neurovascular bundles (D, Control; E, MetSyn). Mesenteric arcade expression of iNOS and CCL2 in control and MetSyn rats (F, n=6). Data are presented as Mean ± SEM. 1-way ANOVA * denotes significance at $p < 0.05$.

Author Manuscript Author Manuscript Author Manuscript Author Manuscript

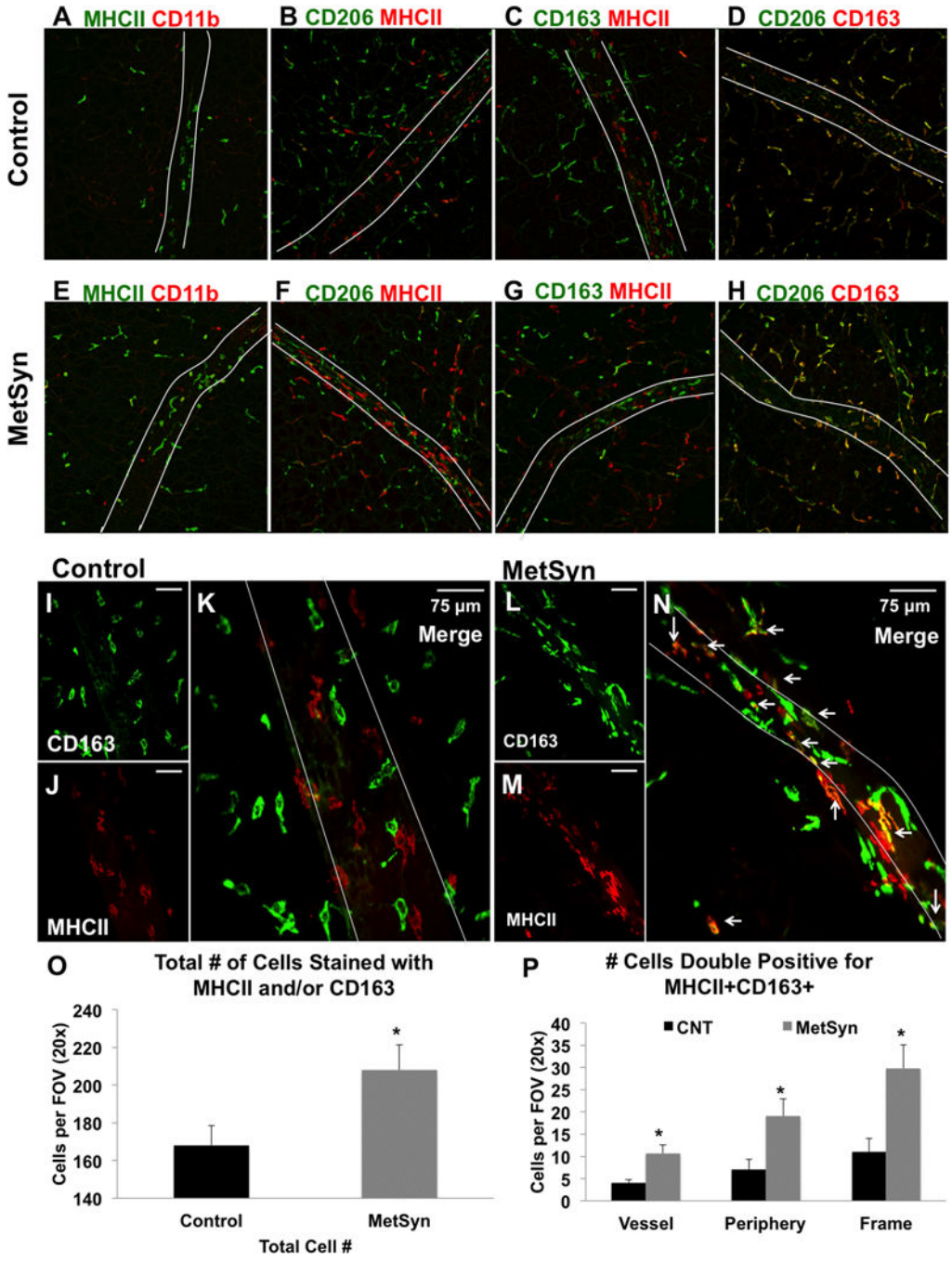

Figure 2.

Macrophage profile in the neurovascular bundles of the mesentery in control and MetSyn rats. Representative images of a 20× field of views dual stained for: MHCII and CD11b A, E), CD206 MHCII (B, F), CD163 MHCII (C, G), and CD206 CD163 (D,H) in both control (A–D) and MetSyn (E-H) mesenteric tissues. B) Representative field of view at 40× magnification of control tissues stained with CD163 (I) and MHCII (J) demonstrate lack of colocalization of the two signals (K). Representative field of view at 40× magnification of MetSyn tissues stained with CD163 (L) and MHCII (M) show increased numbers of

Author Manuscript Author Manuscript Author Manuscript Author Manuscript

immune cells and an increase in double positive (N) cells along the vessel and the periphery. White asterisks in C and F demonstrate $CD163^{+}MHCII^{+}$ cells. The lymphatic vessel is outlined with white lines in each panel. Summary data showing the number of total macrophages stained with MHCII and/or CD163 (O) and the number of double positive $CD163^{+}MHCII^{+}$ cells (P) are shown. Data are presented as Mean ± SEM. N= 6 for each cohort. 2-way ANOVA * denotes significance at $p < 0.05$.

Author Manuscript Author Manuscript Author Manuscript Author Manuscript

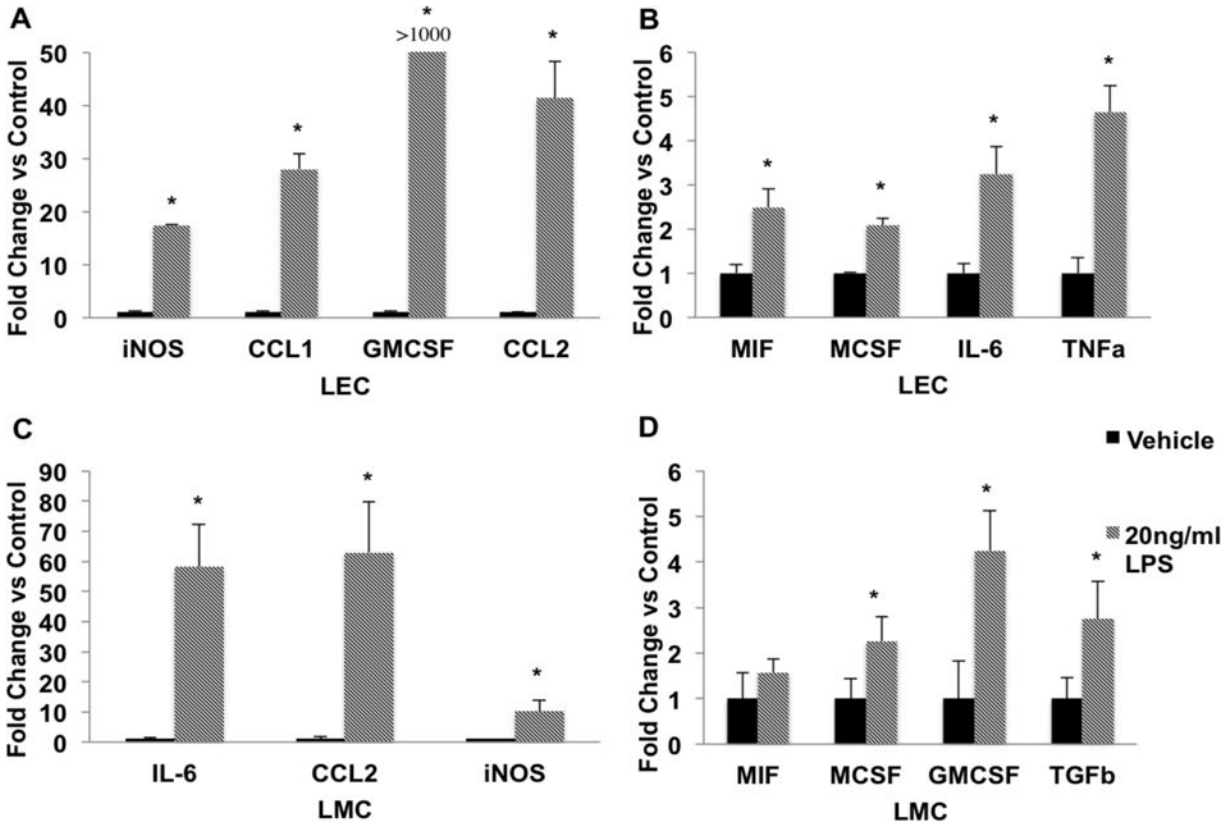

Figure 3.

LPS causes activation of proinflammatory cytokines and chemokines in LECs and LMCs. LECs and LMCs were treated either with PBS (vehicle control) or 20ng/ml LPS for 24 hours. Gene expression was analyzed using the ΔΔCt method as described in the Materials and Methods. A) LECs demonstrated a dramatic increase in the expression of iNOS, CCL1, CCL2, and GMCSF (over 1000 fold) in the LPS-treated group as compared to control group. B) LPS treated LECs also significantly increased expression of MIF, MCSF, IL-6, and TNFα. C) IL-6, CCL2, and iNOS expression was highly up regulated in response to LPS stimulation in LMCs. D) LPS treated LMCs also showed a significant increase in the expression of MIF, MCSF, GMCSF, and TGFβ as compared to the vehicle treated cells. Data are presented as Mean ± SEM. N=3; * denotes significance at $p<0.05$.

Author Manuscript Author Manuscript Author Manuscript Author Manuscript

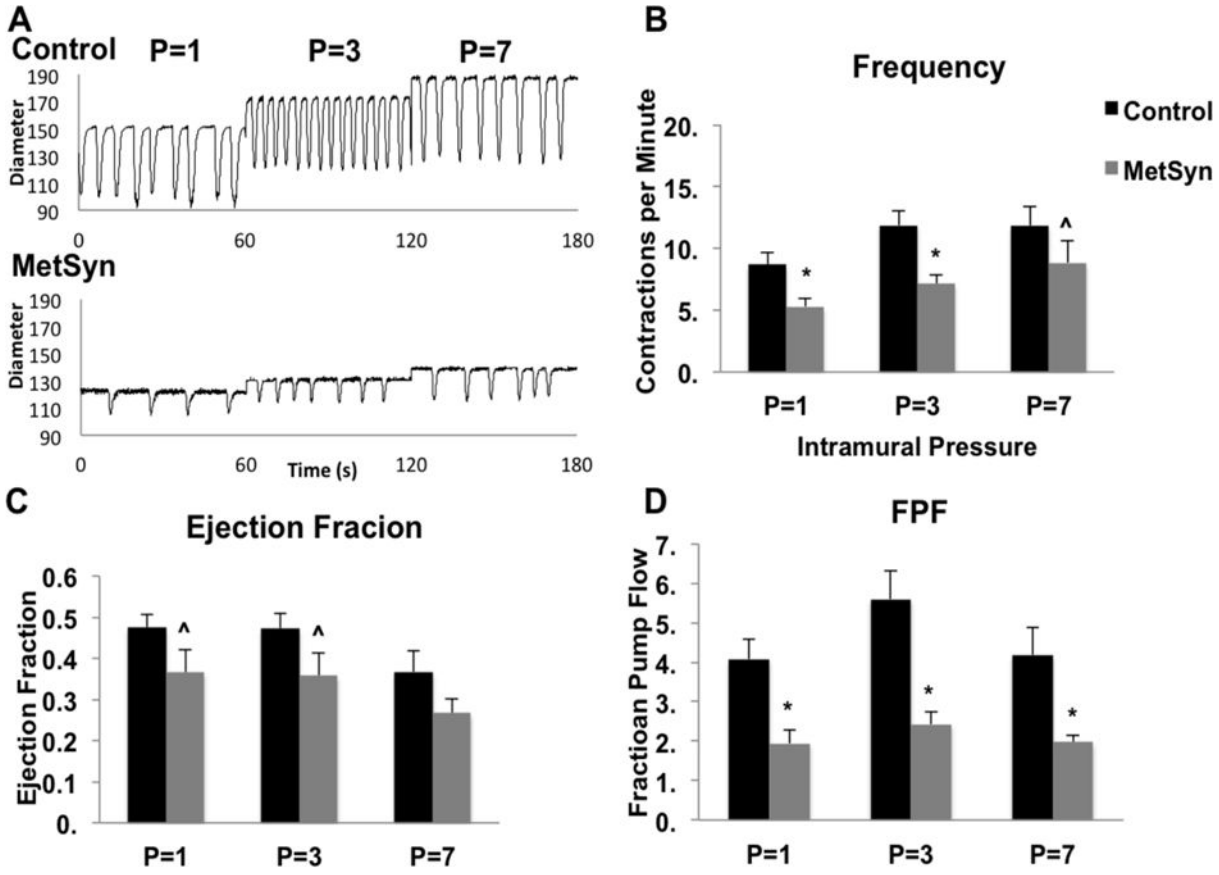

Figure 4.

Lymphatic pump dysfunction in MLVs isolated from MetSyn rats. A) Representative diameter traces over a 1 minute period of control and MetSyn MLVs at each pressure tested. Contraction frequency (B) and ejection fraction (C) for control and MetSyn MLVs. D) Calculated output, fractional pump flow, was significantly lower at all 3 pressures tested. Data are presented as Mean ± SEM. n=8; * denotes significance at $p<0.05$; ˆ denotes significance at $p<0.10$.

Author Manuscript
Author Manuscript
Author Manuscript
Author Manuscript

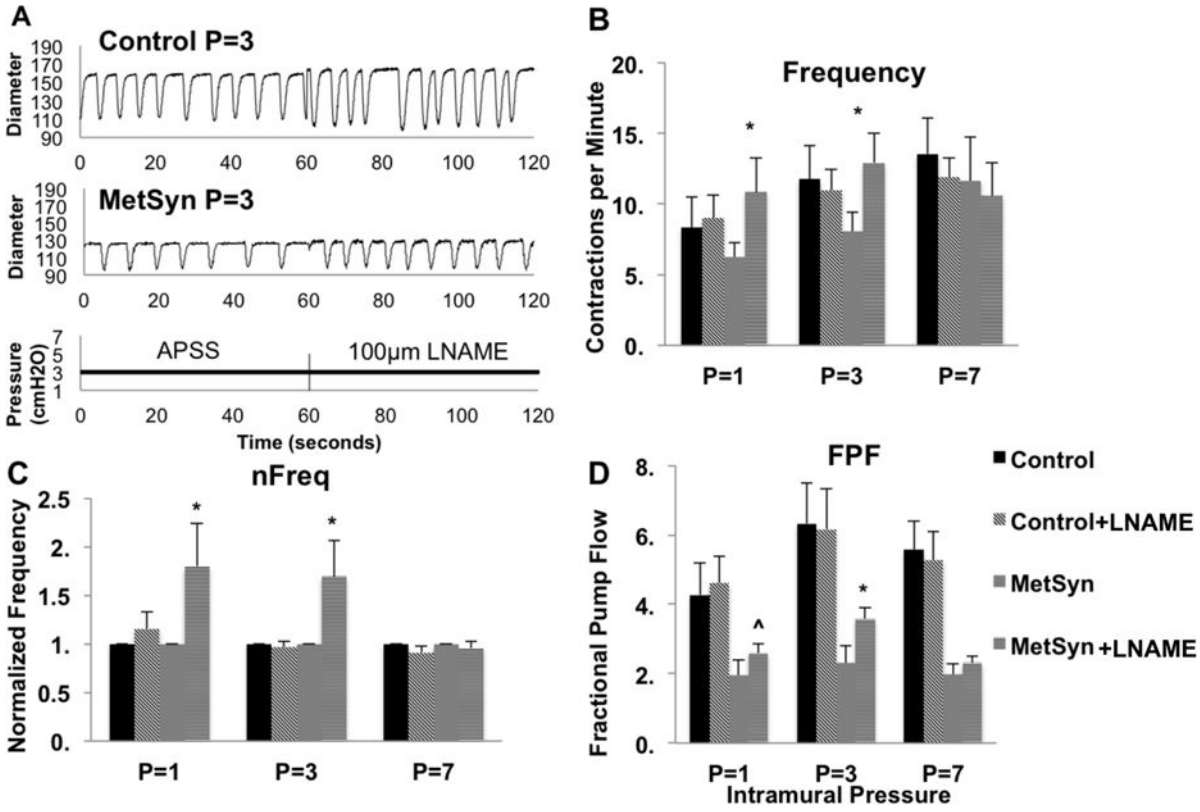

Figure 5.

Inhibition of NOS with 100μm LNAME partially restores MetSyn contractility. A) Representative traces from both control and MetSyn MLVs at pressure 3cmH2O in APSS and in the presence of LNAME. The effect of LNAME on contraction frequency (B), normalized contraction frequency (C), and fractional pump flow (D) in control and MetSyn MLVs. Data are presented as Mean ± SEM n=4. 2-way ANOVA and Fisher post-hoc. * denotes $p<0.05$ LNAME as compared to the respective values in APSS.

Author Manuscript Author Manuscript Author Manuscript Author Manuscript

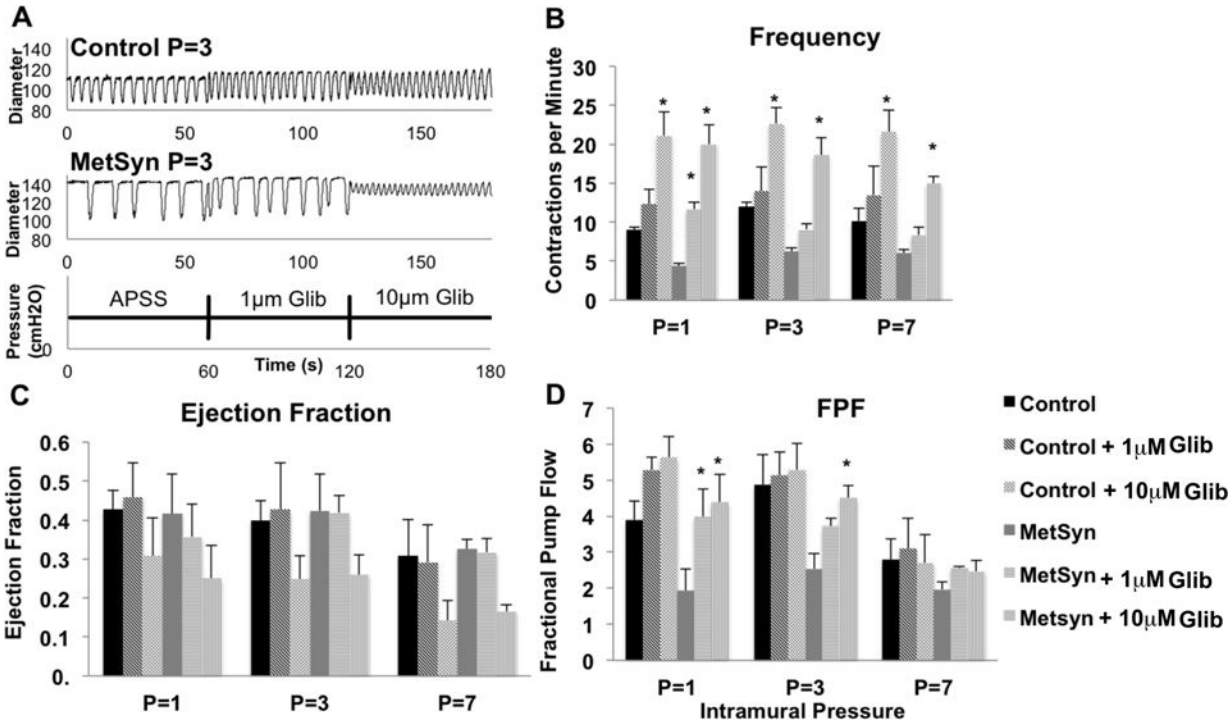

Figure 6.

The effect of Glib on contraction frequency and lymph pump flow in control and MetSyn MLVs. A) Representative traces from both control and MetSyn MLVs at pressure 3cmH2O in APSS, 1um Glib, and 10um Glib. The effect of Glib on contraction frequency (B), ejection fraction (C), and fractional pump flow (D) in control and MetSyn MLVs. Data are presented as Mean ± SEM n=4. 2-way ANOVA and Fisher post-hoc. * denotes $p<0.05$ Glib as compared to the respective values in APSS.

Author Manuscript Author Manuscript Author Manuscript Author Manuscript

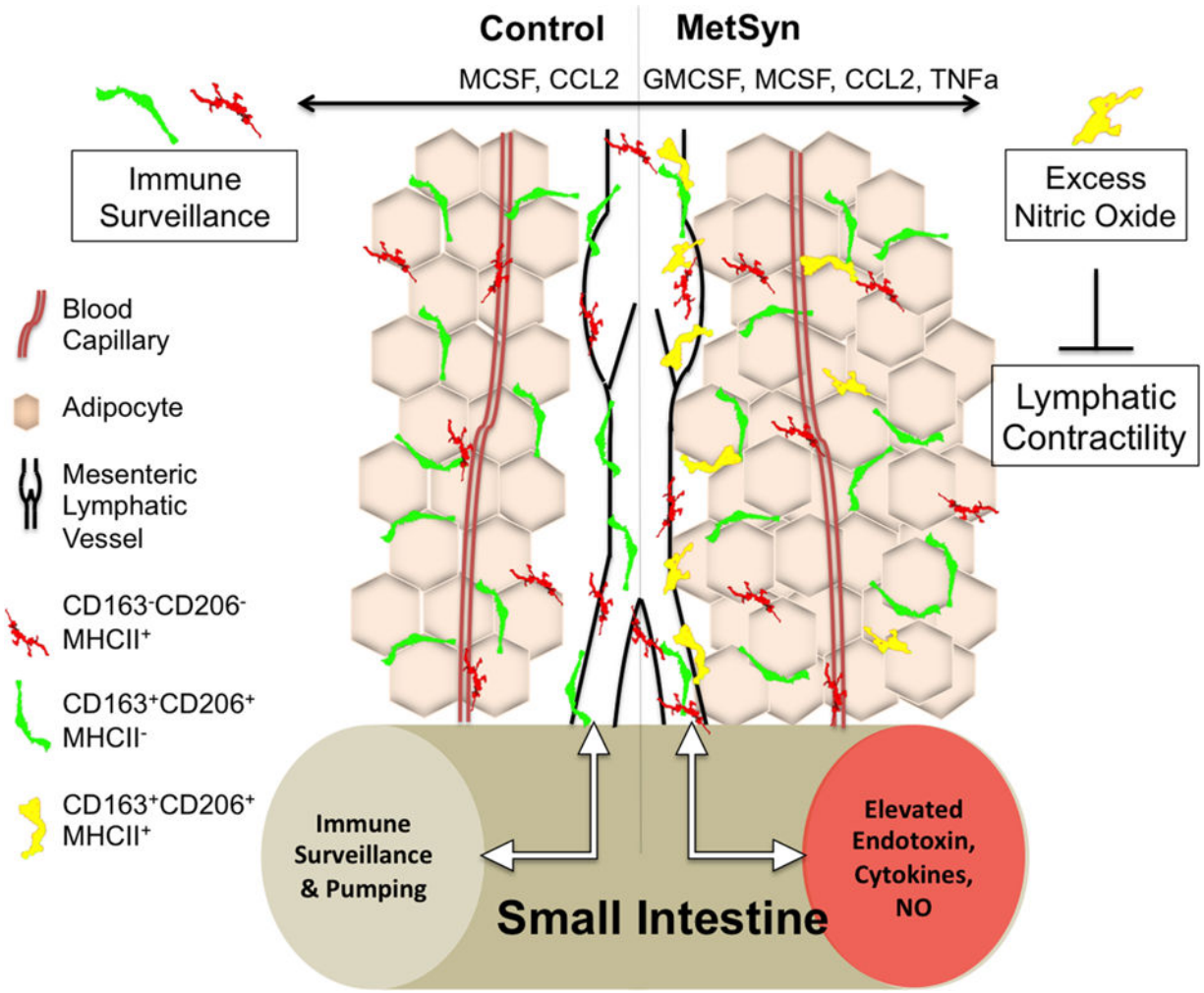

Figure 7.

Model describing the inhibition of lymphatic contractility in the MetSyn as a consequence of inflammation. Mesenteric lymphatic vessels are constantly regulating the flux of inflammatory macrophages into the tissue through MCP1 and MCSF expression. High fructose induces alterations in the gut microbiome and elevations in dietary endotoxin that travels through the mesenteric lymph. Activation of TLR4 on lymphatic tissue results in increased expression of CCL2 and a dramatic up-regulation of GMCSF and recruitment of macrophages into the perivascular tissue and mesenteric collecting lymphatic vessels. Changes in GMCSF, inflammatory cytokines, and dietary endotoxin promote the pro-inflammatory M1 macrophage phenotype and increase iNOS expression.

Author Manuscript Author Manuscript Author Manuscript Author Manuscript

Table 1

Contractile parameters for control and MetSyn MLVs.

Mean ± SEM	Pressure (cm H2O)	P=1	P=3	P=7
Outer Diastolic Diam. (uM)	Control	128 ± 6.50	144 ± 7.4	154 ± 7.9
	MetSyn	120 ± 7.3	134 ± 7.1	144 ± 7.5
Contraction Frequency per Minute	Control	8.7 ± 1.0	11.9 ± 1.1	11.9 ± 1.5
	MetSyn	**5.3 ± 0.6**	**7.2 ± 0.8**	*8.9 ± 1.8*
Ejection Fraction	Control	0.47 ± 0.03	0.47 ± 0.04	0.37 ± 0.05
	MetSyn	*0.37 ± 0.06*	*0.36 ± 0.05*	0.27 ± 0.04
Fractional Pump Flow	Control	4.08 ± 0.50	5.6 ± 0.72	4.18 ± 0.71
	MetSyn	**1.94 ± 0.34**	**2.43 ± 0.30**	**1.98 ± 0.17**
Tonic Index	Control	14.2 ± 2.1	10.4 ± 1.7	8.3 ± 1.8
	MetSyn	12.2 ± 2.3	8.6 ± 1.6	7.4 ± 1.1
Contraction Frequency per Minute	Control L	9.0 ± 1.6	11.0 ± 1.5	11.9 ± 1.4
	Control 1G	12.3 ± 1	14.0 ± 3.1	13.5 ± 3.7
	Control 10G	**21.1 ± 3.0**	**22.7 ± 2.1**	**21.6 ± 2.8**
	MetSyn L	**10.9 ± 2.5**	**12.9 ± 2.1**	10.6 ± 2.4
	MetSyn 1G	**11.7 ± 0.9**	9.1 ± 0.8	8.3 ± 1.0
	MetSyn 10G	**20.0 ± 2.5**	**18.6 ± 2.3**	**15.0 ± 0.9**
Ejection Fraction	Control L	0.52 ± 0.05	0.56 ± 0.04	0.45 ± 0.05
	Control 1G	0.46 ± 0.1	0.43 ± 0.14	0.29 ± 0.11
	Control 10G	0.31 ± 0.10	0.25 ± 0.06	*0.14 ± 0.05*
	MetSyn L	0.28 ± 0.07	0.30 ± 0.06	0.28 ± 0.1
	MetSyn 1G	0.36 ± 0.1	0.42 ± 0.05	0.32 ± 0.04
	MetSyn 10G	0.25 ± 0.08	0.26 ± 0.05	0.17 ± 0.02
Fractional Pump Flow	Control L	4.61 ± 0.77	6.16 ± 1.16	5.27 ± 0.82
	Control 1G	5.29 ± 0.35	5.13 ± 0.65	3.09 ± 0.84
	Control 10G	5.63 ± 0.58	5.28 ± 0.72	2.70 ± 0.78
	MetSyn L	**2.59 ± 0.27**	**3.58 ± 0.31**	2.31 ± 0.19
	MetSyn 1G	**3.98 ± 0.78**	3.71 ± 0.22	2.56 ± 0.04
	MetSyn 10G	**4.39 ± 0.77**	**4.51 ± 0.35**	2.47 ± 0.31
Tonic Index	Control L	14.8 ± 2.5	9.2 ± 2.1	8.8 ± 2.4
	Control 1G	8.7 ± 2.9	7.4 ± 1.9	5.2 ± 1.7
	Control 10G	10.9 ± 2.9	7.6 ± 0.9	6.0 ± 1.8
	MetSyn L	10.8 ± 1.5	8.4 ± 1.9	6.3 ± 1.5
	MetSyn 1G	9.8 ± 4.0	6.4 ± 0.9	4.6 ± 0.4
	MetSyn 10G	16.2 ± 1.9	7.7 ± 1.2	5.2 ± 0.4